# Supplement to
# Upper tropospheric slightly ice-subsaturated regions: Frequency of occurrence and statistical evidence for the appearance of contrail cirrus

Yun Li[1,2], Christoph Mahnke[1], Susanne Rohs[1], Ulrich Bundke[1], Nicole Spelten[2], Georgios Dekoutsidis[3], Silke Groß[3], Christiane Voigt[3,4], Ulrich Schumann[3], Andreas Petzold[1] and Martina Krämer[2,4]

[1]Forschungszentrum Jülich, Institute of Energy and Climate Research – Troposphere (IEK-8), Jülich, Germany
[2]Forschungszentrum Jülich, Institute of Energy and Climate Research – Stratosphere (IEK-7), Jülich, Germany
[3]Deutsches Zentrum für Luft- und Raumfahrt (DLR), Institut für Physik der Atmosphäre, Oberpfaffenhofen, Germany
[4]Johannes Gutenberg-Universität, Institute of Atmospheric Physics, Mainz, Germany

*Correspondence to*: Yun Li (yun.li@fz-juelich.de) and Martina Krämer (m.kraemer@fz-juelich.de)

This Supplement contains an additional table complementing the ML-CIRRUS dataset introduced in Sect. 2 and extra figures supporting the interpretation of our results presented in Sect. 3 of the paper. Details about the table and each figure can be found in the corresponding sections of the paper as mentioned in the supplement figure captions.

**Contents**

**Table S1.** Twelve scientific flights from the ML-CIRRUS 2014 campaign that contain a complete dataset of ice cloud parameters are selected for the study of the microphysical properties and occurrences of contrail and natural cirrus. The table is adapted from Table 3 in Voigt et al. (2017). The cloud particle sampling frequency is 1 Hz during flights. See Sect. 2.1 in the paper for details.

| Flight Nr. | Date | Mission of single flights | Flight area | Flight hours |
|---|---|---|---|---|
| 1, 2 | March 22 a, b | Test flights | Germany | 6 hrs |
| 3 | March 26 | contrails and contrail cirrus | North Atlantic flight corridor | 8. 5 hrs |
| 4 | March 27 | Fronts and warm conveyor belts (WCBs) induced cirrus | Alps, Italy, and Germany | 4.75 hrs |
| 5 | March 29 | Cirrus induced by dynamics, *e.g.*, fronts, convection, *etc*. | France and Spain | 7.5 hrs |
| 6 | April 1 | Cirrus, contrail cirrus | Germany | 6.58 hrs |
| 7 | April 3 | Cirrus from WCBs outflow | Germany | 5.25 hrs |
| 8 | April 7 | Contrail cirrus | Germany | 5.58 hrs |
| 9 | April 10 | contrails and contrail cirrus | Germany | 3.25 hrs |
| 10, 11 | April 11 a, b | Cirrus from fronts and WCBs | Great Britain | 10 hrs |
| 12 | April 13 | Cirrus in high pressure system and jet stream | France, Spain, Portugal | 3 hrs |
| | | | Total flight hours: | 60.4 hrs |
| | | | Valid data volume in hours: | 48.5 hrs |
| | | | Valid cirrus sampling hours: | 14.7 hrs |

## S1 In situ-origin contrail cirrus and liquid-origin natural cirrus

In situ-origin cirrus means that the cirrus ice crystals have formed and grown in an ice cloud only environment, while liquid-origin cirrus refers to the cirrus whose ice crystals originally form as liquid drops in a warmer atmosphere ($T_{amb}$ > 235 K), which subsequently freeze while being lifted into the cirrus temperature region of the atmosphere. In situ-origin cirrus are often associated with small ice particles with low ice water content. In contrast, liquid-origin cirrus tends to yield large ice crystals with higher ice water content IWC. See Luebke et al. (2016) and Krämer et al. (2016; 2020) for more details.

From Fig. S1 a and b, we can see that the high occurrences of IWC are in the lower IWC range (< 10 parts per million by cirrus (3.99 hrs out of 4.01 hours in Fig. 5a) are formed in situ. Over two-thirds of the natural cirrus (Fig. 4b) are liquid-liquid origin cirrus, as shown in Fig. S1 c and d.

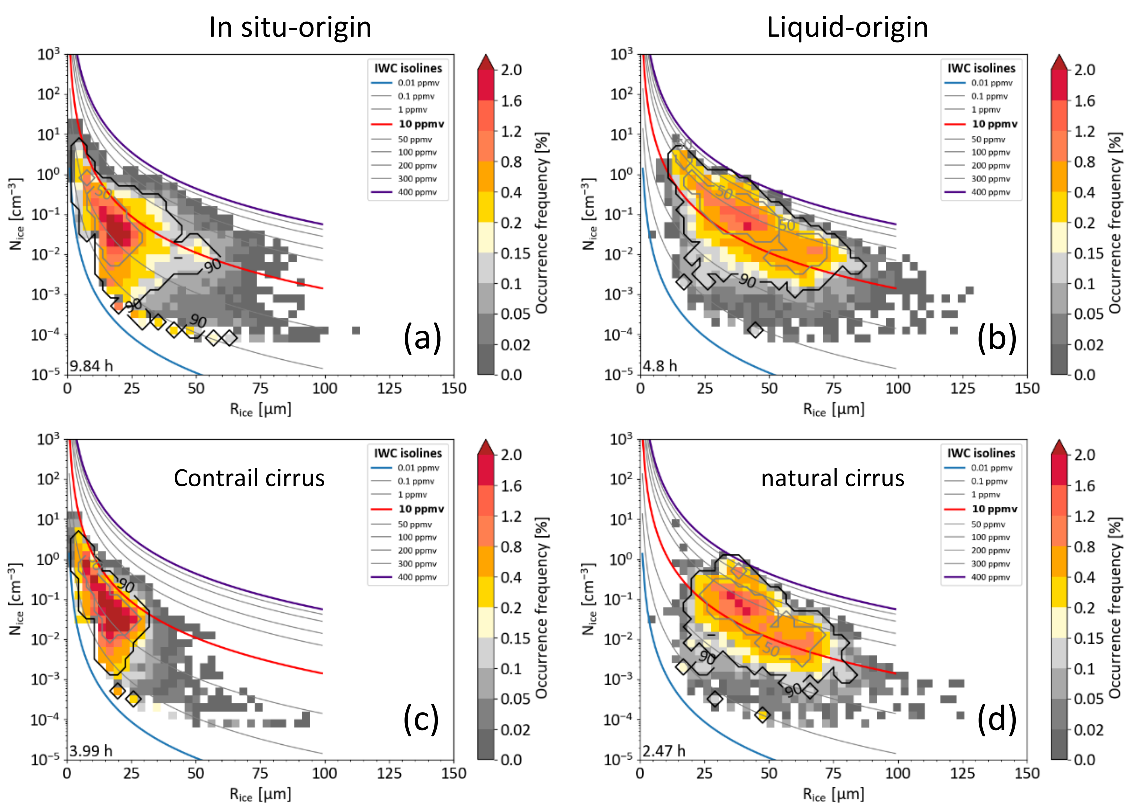


**Figure S1.** Ice crystal number concentration $N_{ice}$ in relation to mass mean radius $R_{ice}$ for the in situ-origin (left) and liquid-origin cirrus (right) sampled during the ML-CIRRUS 2014 campaign. Coloured curves in the figures are ice water content IWC isolines in parts per million by volume (ppmv). The same amount of IWC could consist of many small ice particles pointing to the upper-left end of the isoline or few large ice crystals in the lower-right end. The size of each dataset in flight hours at 1 Hz sapling frequency is added to the lower right corner of each figure. The grey and black contours enclose 50% and 90% of the most frequent ice particles. (a): $N_{ice}$–$R_{ice}$ relation for all in situ-origin cirrus (medians $R_{ice}$ = 0.03 $cm^{-3}$, $N_{ice}$ = 20 µm). (b): $N_{ice}$–$R_{ice}$ relation for all liquid-origin cirrus (medians $R_{ice}$ = 0.05 $cm^{-3}$, $N_{ice}$ = 42 µm). (c): $N_{ice}$–$R_{ice}$ relation for all contrail cirrus of in situ-origin (medians: $R_{ice}$ = 0.04 $cm^{-3}$, $N_{ice}$ = 17 µm). The contrail cirrus is identified with the Schmidt-Appleman criterion (SAC) and the frequent aircraft cruising altitude range (CA, ambient pressure 200–245 hPa). (d): $N_{ice}$–$R_{ice}$ relation for all natural cirrus of liquid-origin (medians: $R_{ice}$ = 0.02 $cm^{-3}$, $N_{ice}$ = 45 µm). The natural cirrus does not fulfil SAC and CA. See Sect. 3.1 in the paper for details.

### S2 Slight ice-subsaturation in contrail cirrus

Contrail cirrus is identified by combining the Schmidt-Appleman criterion (SAC, calculated using water vapour emission index, aircraft fuel properties and engine efficiency, see text and Schumann (1996) and the most frequent aircraft cruising altitude range (CA, ambient pressure range 200–245 hPa, ambient temperature range 208–217 K). Contrail cirrus fulfilling SAC and located inside the CA range are shown in Fig. S2b, while natural cirrus missing SAC and CA are shown in Fig. S2c. The color coding shows the relative humidity with respect to ice $RH_{ice}$ in cirrus clouds, revealing that contrail cirrus are mostly subsaturated with respect to ice, with the $RH_{ice}$ around 90% in the area of mass mean radius $R_{ice}$ < 20 µm and ice crystal number concentration $N_{ice}$ > 0.05 $cm^{-3}$. High $RH_{ice}$ are more frequently found in the thin in situ-origin cirrus of which both $N_{ice}$ and IWC are small or in the liquid-origin cirrus of more larger ice crystals and high IWC.

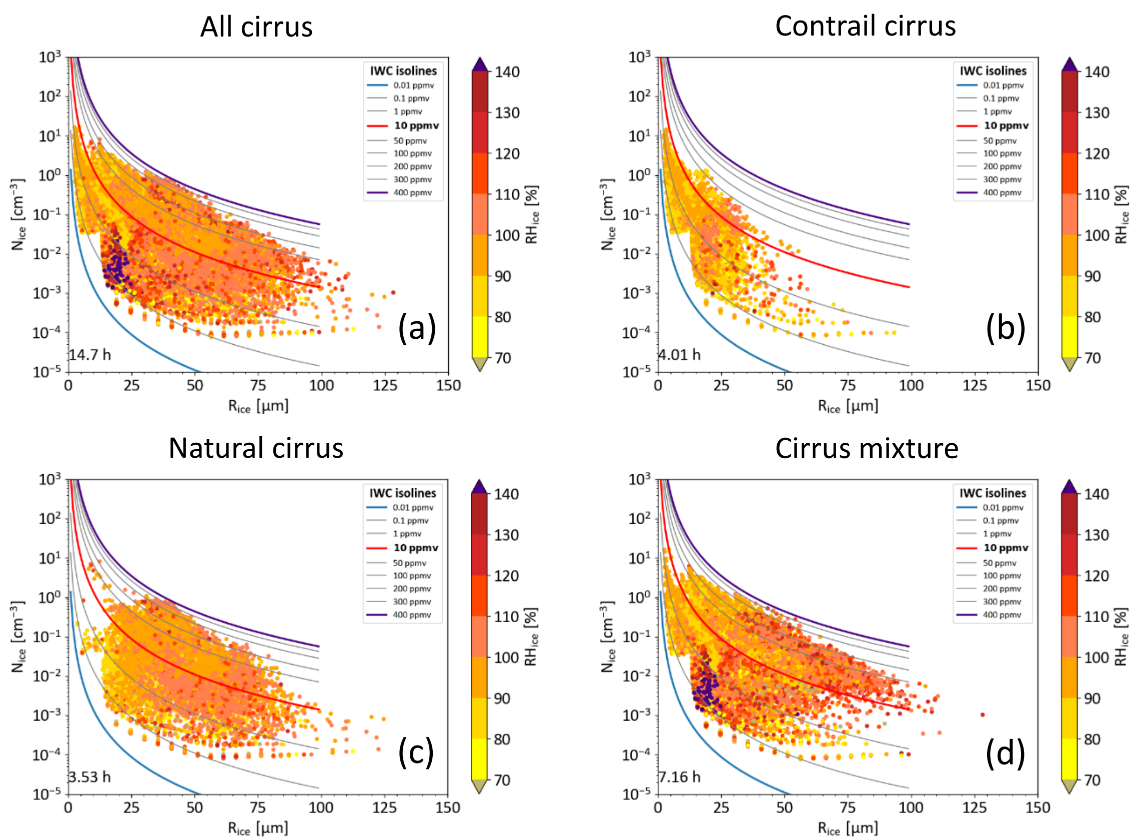


**Figure S2.** Scatter plots of ice crystal number concentration $N_{ice}$ dependent of mass mean radius $R_{ice}$ in all cirrus clouds (a), the contrail cirrus (b), the natural cirrus (c) and the cirrus mixture (d) sampled during the ML-CIRRUS campaign. Coloured curves in the figures are ice water content IWC isolines in parts per million by volume (ppmv). The same amount of IWC could come from many small ice particles pointing to the upper-left end of the isoline or few large ice crystals in the lower-right end. The size of each dataset in flight hours at 1 Hz sapling frequency is added to the lower left corner of each figure. See Sect. 3.2.1 in the paper for details.

## S3 The robustness of the in situ $RH_{ice}$ in relation to the ambient temperature uncertainty

Determination of in situ $RH_{ice}$ values is based on the water vapour measurement of the SHARC hygrometer and the ambient temperature $T_{amb}$ and pressure measured by the Basis Halo Measurement and Sensor System (BAHAMAS). The nominal accuracies of the BAHAMAS $T_{amb}$ and pressure measurement are 0.3 hPa and 0.5 K. There could be a small bias in the in situ $RH_{ice}$ dataset due to a bias in the BAHAMAS $T_{amb}$ measurement as indicated by and Schumann (2021; See page 108). To evaluate the changes of in situ $RH_{ice}$ values which could be caused by the temperature uncertainty and to check the robustness of our results, we introduced a negative $T_{amb}$ bias of 0.5 K and recalculated the saturation pressure over ice at ($T_{amb}$–0.5) K based on Murphy and Koop (2005) and the in situ $RH_{ice}$.

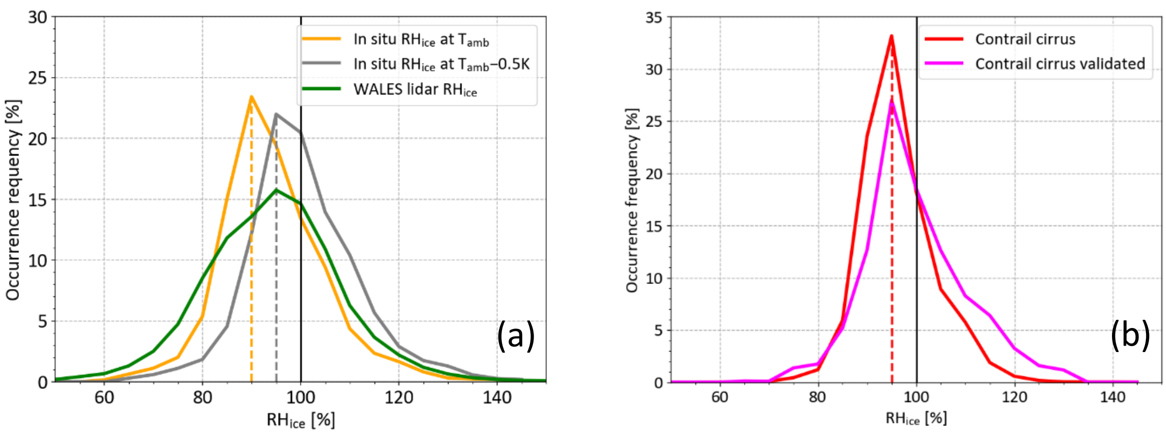


**Figure S3.** (a): Normalised $RH_{ice}$ occurrence frequency in 5% $RH_{ice}$ bins. The orange curve shows the in situ $RH_{ice}$ distribution with the currently used ambient temperature $T_{amb}$ values provided by the HALO database (https://halo-db.pa.op.dlr.de/). The grey curve exhibits the in situ $RH_{ice}$ distribution with a subtraction of 0.5 K from the currently used Tamb values. The frequency distribution of the Lidar $RH_{ice}$ measured by the remote sensing instrument WALES on board is shown as the green curve. (b): Normalised $RH_{ice}$ occurrence frequency in 5% $RH_{ice}$ bins with $T_{amb}$ subtracted by 0.5 K for the contrail cirrus (in red) fulfilling the Schmidt-Appleman criterion (SAC) and inside the cruising altitude range (CA) and for the contrail cirrus validated with the plume detection method (fulfilling SAC and the CA range not applied) (in magenta). See Sect. 3.3 in the paper for details.

Figure S3a shows the normalised in-cloud $RH_{ice}$ occurrence frequency distribution in all cirrus clouds from the currently used $T_{amb}$ dataset and from the adjusted temperature dataset by subtracting 0.5 K. In addition, the in-cloud $RH_{ice}$ distribution obtained by the lidar WALES is plotted in the figure. We can see, on one hand, that introducing a negative temperature bias of 0.5 K makes the peak of the $RH_{ice}$ distribution shift from 90% $RH_{ice}$ under the current $T_{amb}$ dataset to 95% $RH_{ice}$, which is at the peak of the lidar $RH_{ice}$. However, when a constant bias is assumed, the whole distribution of $RH_{ice}$ at ($T_{amb}$–0.5) K is shifted rightwards in comparison to the lidar $RH_{ice}$ distribution. The in situ $RH_{ice}$ distribution derived from the current $T_{amb}$ dataset agrees better with the $RH_{ice}$ distribution from the lidar measurements, considering the $RH_{ice}$ ranges at the full width half maxima and the $RH_{ice}$ ranges with the most frequent $RH_{ice}$ occurrence (>80%). Figure S3b displays the normalised frequency distributions of the contrail cirrus (fulfilling SAC and inside CA) and the contrail cirrus that are validated using the plume detection algorithm (fulfilling SAC and CA not applied), at ($T_{amb}$–0.5) K. The highest occurrence frequency in both contrail cirrus identified using SAC-CA combination and by applying the plume detection method is still in slight ice subsaturation (95%). Concluding, we consider the current $T_{amb}$ dataset, as has been applied in many previous publications, see *e.g.*, the ACP/AMT inter-journal Special Issue: ML-CIRRUS – the airborne experiment on natural cirrus and contrail cirrus in mid-latitudes with the high-altitude long-range research aircraft HALO (https://acp.copernicus.org/articles/special_issue820.html), and specifically Kaufmann et al. (2018); Krämer et al. (2020); Luebke et al. (2016); Schumann et al. (2017); Voigt et al. (2017), as applicable within the specified uncertainties.

**References**

Kaufmann, S., Voigt, C., Heller, R., Jurkat-Witschas, T., Krämer, M., Rolf, C., Zöger, M., Giez, A., Buchholz, B., Ebert, V., Thornberry, T., and Schumann, U.: Intercomparison of midlatitude tropospheric and lower-stratospheric water vapor measurements and comparison to ECMWF humidity data, Atmos. Chem. Phys., 18, 16729-16745, https://doi.org/10.5194/acp-18-16729-2018, 2018.

Krämer, M., Rolf, C., Spelten, N., Afchine, A., Fahey, D., Jensen, E., Khaykin, S., Kuhn, T., Lawson, P., Lykov, A., Pan, L. L., Riese, M., Rollins, A., Stroh, F., Thornberry, T., Wolf, V., Woods, S., Spichtinger, P., Quaas, J., and Sourdeval, O.: A microphysics guide to cirrus – Part 2: Climatologies of clouds and humidity from observations, Atmos. Chem. Phys., 20, 12569-12608, https://doi.org/10.5194/acp-20-12569-2020, 2020.

Luebke, A. E., Afchine, A., Costa, A., Grooß, J. U., Meyer, J., Rolf, C., Spelten, N., Avallone, L. M., Baumgardner, D., and Krämer, M.: The origin of midlatitude ice clouds and the resulting influence on their microphysical properties, Atmos. Chem. Phys., 16, 5793-5809, https://doi.org/10.5194/acp-16-5793-2016, 2016.

Murphy, D. M. and Koop, T.: Review of the vapour pressures of ice and supercooled water for atmospheric applications, Q. J. R. Meteorol. Soc., 131, 1539-1565, https://doi.org/10.1256/qj.04.94, 2005.

Schumann, U.: On conditions for contrail formation from aircraft exhausts, Meteorol. Z., 5, 4-23, https://doi.org/10.1127/metz/5/1996/4, 1996.

Schumann, U.: Measurement and model data comparisons for the HALO-FAAM formation flight during EMeRGe on 17 July 2017, https://doi.org/10.5281/zenodo.4427965, 2021.

Schumann, U., Baumann, R., Baumgardner, D., Bedka, S. T., Duda, D. P., Freudenthaler, V., Gayet, J. F., Heymsfield, A. J., Minnis, P., Quante, M., Raschke, E., Schlager, H., Vázquez-Navarro, M., Voigt, C., and Wang, Z.: Properties of individual contrails: a compilation of observations and some comparisons, Atmos. Chem. Phys., 17, 403-438, https://doi.org/10.5194/acp-17-403-2017, 2017.

Voigt, C., Schumann, U., Minikin, A., Abdelmonem, A., Afchine, A., Borrmann, S., Boettcher, M., Buchholz, B., Bugliaro, L., Costa, A., Curtius, J., Dollner, M., Dörnbrack, A., Dreiling, V., Ebert, V., Ehrlich, A., Fix, A., Forster, L., Frank, F., Fütterer, D., Giez, A., Graf, K., Grooß, J.-U., Groß, S., Heimerl, K., Heinold, B., Hüneke, T., Järvinen, E., Jurkat, T., Kaufmann, S., Kenntner, M., Klingebiel, M., Klimach, T., Kohl, R., Krämer, M., Krisna, T. C., Luebke, A., Mayer, B., Mertes, S., Molleker, S., Petzold, A., Pfeilsticker, K., Port, M., Rapp, M., Reutter, P., Rolf, C., Rose, D., Sauer, D., Schäfler, A., Schlage, R., Schnaiter, M., Schneider, J., Spelten, N., Spichtinger, P., Stock, P., Walser, A., Weigel, R., Weinzierl, B., Wendisch, M., Werner, F., Wernli, H., Wirth, M., Zahn, A., Ziereis, H., and Zöger, M.: ML-CIRRUS: The Airborne Experiment on Natural Cirrus and Contrail Cirrus with the High-Altitude Long-Range Research Aircraft HALO, Bull. Amer. Meteor. Soc., 98, 271-288, https://doi.org/10.1175/BAMS-D-15-00213.1, 2017.